

Original citation:

LHCb Collaboration (Including: Back, John J., Craik, Daniel, Dossett, D., Gershon, Timothy J., Kreps, Michal, Latham, Thomas, Pilar, T., Poluektov, Anton, Reid, Matthew M., Silva Coutinho, R., Wallace, Charlotte, Whitehead, M. (Mark) and Williams, M. P.). (2014) Search for the decay $D^0 \rightarrow \pi^+ \pi^- \mu^+ \mu^-$. Physics Letters B, Volume 728 . pp. 234-243.

Permanent WRAP url:

<http://wrap.warwick.ac.uk/59628>

Copyright and reuse:

The Warwick Research Archive Portal (WRAP) makes this work of researchers of the University of Warwick available open access under the following conditions.

This article is made available under the Creative Commons Attribution- 3.0 Unported (CC BY 3.0) license and may be reused according to the conditions of the license. For more details see <http://creativecommons.org/licenses/by/3.0/>

A note on versions:

The version presented in WRAP is the published version, or, version of record, and may be cited as it appears here.

For more information, please contact the WRAP Team at: publications@warwick.ac.uk

warwick**publications**wrap

highlight your research

<http://wrap.warwick.ac.uk/>



Search for the decay $D^0 \rightarrow \pi^+\pi^-\mu^+\mu^-$ [☆]



LHCb Collaboration

ARTICLE INFO

Article history:

Received 9 October 2013
 Received in revised form 14 November 2013
 Accepted 24 November 2013
 Available online 28 November 2013
 Editor: M. Doser

ABSTRACT

A search for the $D^0 \rightarrow \pi^+\pi^-\mu^+\mu^-$ decay, where the muon pair does not originate from a resonance, is performed using proton–proton collision data corresponding to an integrated luminosity of 1.0 fb^{-1} recorded by the LHCb experiment at a centre-of-mass energy of 7 TeV. No signal is observed and an upper limit on the relative branching fraction with respect to the resonant decay mode $D^0 \rightarrow \pi^+\pi^-\phi(\rightarrow \mu^+\mu^-)$, under the assumption of a phase-space model, is found to be

$$\mathcal{B}(D^0 \rightarrow \pi^+\pi^-\mu^+\mu^-)/\mathcal{B}(D^0 \rightarrow \pi^+\pi^-\phi(\rightarrow \mu^+\mu^-)) < 0.96$$

at 90% confidence level. The upper limit on the absolute branching fraction is evaluated to be $\mathcal{B}(D^0 \rightarrow \pi^+\pi^-\mu^+\mu^-) < 5.5 \times 10^{-7}$ at 90% confidence level. This is the most stringent to date.

© 2013 The Authors. Published by Elsevier B.V. All rights reserved.

1. Introduction

Flavour-changing neutral current (FCNC) processes are rare within the Standard Model (SM) as they cannot occur at tree level and are suppressed by the Glashow–Iliopoulos–Maiani (GIM) mechanism at loop level. In contrast to the B meson system, where the high mass of the top quark in the loop weakens the suppression, the GIM cancellation is almost exact [1] in D meson decays, leading to expected branching fractions for $c \rightarrow u\mu^+\mu^-$ processes in the range $(1-3) \times 10^{-9}$ [2–4]. This suppression allows for sub-leading processes with potential for physics beyond the SM, such as FCNC decays of D mesons, and the coupling of up-type quarks in electroweak processes illustrated in Fig. 1, to be probed more precisely.

The total branching fraction for these decays is expected to be dominated by long-distance contributions involving resonances, such as $D^0 \rightarrow \pi^+\pi^-V(\rightarrow \mu^+\mu^-)$, where V can be any of the light vector mesons ϕ , ρ^0 or ω . The corresponding branching fractions can reach $\mathcal{O}(10^{-6})$ [2–4]. The angular structure of these four-body semileptonic D^0 decays provides access to a variety of differential distributions. Of particular interest are angular asymmetries that allow for a theoretically robust separation of long- and short-distance effects, the latter being more sensitive to physics beyond the SM [4]. No such decays have been observed to date and the most stringent limit reported is $\mathcal{B}(D^0 \rightarrow \pi^+\pi^-\mu^+\mu^-) < 3.0 \times 10^{-5}$ at 90% confidence level (CL) by the E791 Collaboration [5]. The same processes can be probed using $D_{(s)}^+ \rightarrow \pi^+\mu^+\mu^-$ decays.

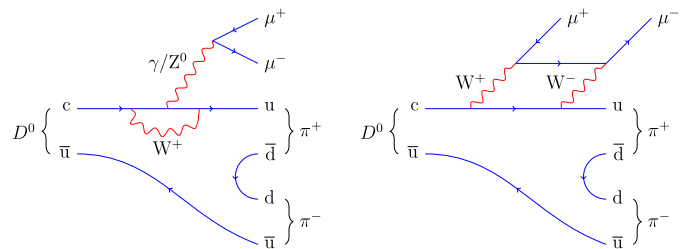


Fig. 1. Leading Feynman diagrams for the FCNC decay $D^0 \rightarrow \pi^+\pi^-\mu^+\mu^-$ in the SM.

Upper limits on their branching fractions have been recently set to $\mathcal{B}(D^+ \rightarrow \pi^+\mu^+\mu^-) < 7.3 \times 10^{-8}$ and $\mathcal{B}(D_s^+ \rightarrow \pi^+\mu^+\mu^-) < 4.1 \times 10^{-7}$ at 90% CL by the LHCb Collaboration [6].

This Letter presents the result of a search for the $D^0 \rightarrow \pi^+\pi^-\mu^+\mu^-$ decay, in which the muons do not originate from a resonance, performed using $D^{*+} \rightarrow D^0\pi^+$ decays, with the D^{*+} meson produced directly at the pp collision primary vertex. The reduction in background yield associated with this selection vastly compensates for the loss of signal yield. No attempt is made to distinguish contributions from intermediate resonances in the dipion invariant mass such as the ρ^0 . Throughout this Letter, the inclusion of charge conjugate processes is implied. The data samples used in this analysis correspond to an integrated luminosity of 1.0 fb^{-1} at $\sqrt{s} = 7 \text{ TeV}$ recorded by the LHCb experiment.

The analysis is performed in four dimuon mass ranges to exclude decays dominated by the contributions of resonant dimuon final states. The regions at low and high dimuon masses, away from the η , ρ^0 and ϕ resonant regions, are the most sensitive to non-SM physics and are defined as the signal regions. The signal yield is normalised to the yield of resonant

[☆] This is an open-access article distributed under the terms of the Creative Commons Attribution License, which permits unrestricted use, distribution, and reproduction in any medium, provided the original author and source are credited. Funded by SCOAP³.

$D^0 \rightarrow \pi^+\pi^-\phi (\rightarrow \mu^+\mu^-)$ decays, isolated in an appropriate dimuon range centred around the ϕ pole.

2. The LHCb detector and trigger

The LHCb detector [7] is a single-arm forward spectrometer covering the pseudorapidity range $2 < \eta < 5$, designed for the study of particles containing b or c quarks. The detector includes a high-precision tracking system consisting of a silicon-strip vertex detector surrounding the pp interaction region, a large-area silicon-strip detector located upstream of a dipole magnet with a bending power of about 4 Tm, and three stations of silicon-strip detectors and straw drift tubes placed downstream. The combined tracking system provides a momentum measurement with relative uncertainty that varies from 0.4% at 5 GeV/c to 0.6% at 100 GeV/c, and impact parameter resolution of 20 μm for tracks with large transverse momentum. Different types of charged hadrons are distinguished by information from two ring-imaging Cherenkov detectors [8]. Photon, electron and hadron candidates are identified by a calorimeter system consisting of scintillating-pad and preshower detectors, an electromagnetic calorimeter and a hadronic calorimeter. Muons are identified by a system composed of alternating layers of iron and multiwire proportional chambers [9].

The trigger [10] consists of a hardware stage, based on information from the calorimeter and muon systems, followed by a software stage, which applies a full event reconstruction. The hardware trigger selects muons with transverse momentum, p_T , exceeding 1.48 GeV/c, and dimuons whose product of p_T values exceeds $(1.3 \text{ GeV}/c)^2$. In the software trigger, at least one of the final state muons is required to have momentum larger than 8 GeV/c, and to have an impact parameter, IP, defined as the minimum distance of the particle trajectory from the associated primary vertex (PV) in three dimensions, greater than 100 μm . Alternatively, a dimuon trigger accepts events with oppositely charged muon candidates having good track quality, p_T exceeding 0.5 GeV/c, and momentum exceeding 6 GeV/c. In a second stage of the software trigger, two algorithms select $D^0 \rightarrow \pi^+\pi^-\mu^+\mu^-$ candidates. The first algorithm, used to increase the efficiency in the highest dimuon mass region, requires oppositely charged muons with scalar sum of p_T greater than 1.5 GeV/c and dimuon mass greater than 1 GeV/c^2 . A second algorithm selects events with two oppositely charged muons and two oppositely charged hadrons with no invariant mass requirement on the dimuon.

Simulated events for the signal, using a phase-space model, and the normalisation mode, are used to define selection criteria and to evaluate efficiencies. The pp collisions are generated using PYTHIA 6.4 [11] with a specific LHCb configuration [12]. Decays of hadronic particles are described by EVTGEN [13]. The interaction of the generated particles with the detector and its response are implemented using the GEANT4 toolkit [14,15] as described in Ref. [16].

3. Candidate selection

Candidate $D^0 \rightarrow \pi^+\pi^-\mu^+\mu^-$ decays are required to originate from $D^{*+} \rightarrow D^0\pi^+$ decays. The D^0 candidate is formed by combining two pion and two muon candidates where both pairs consist of oppositely charged particles. An additional pion track is combined with the D^0 candidate to build the D^{*+} candidate. The χ^2 per degree of freedom of the vertex fit is required to be less than 5 for both the D^{*+} and the D^0 candidates. The angle between the D^0 momentum vector and the direction from the associated PV to the decay vertex, θ_{D^0} , is required to be less than 0.8° . Each of the four particles forming the D^0 meson must have momentum

exceeding 3 GeV/c and p_T exceeding 0.4 GeV/c. The tracks must be displaced with respect to any PV and have χ_{IP}^2 larger than 4. Here χ_{IP}^2 is defined as the difference between the χ^2 of the PV fit done with and without the track under consideration.

Further discrimination is achieved using a boosted decision tree (BDT) [17–19], which distinguishes between signal and combinatorial background candidates. This multivariate analysis algorithm is trained using simulated $D^0 \rightarrow \pi^+\pi^-\mu^+\mu^-$ signal events and a background sample taken from data mass sidebands around the $D^0 \rightarrow \pi^+\pi^-\mu^+\mu^-$ signal mass region. Only 1% of the candidates in the sidebands are used in the training. The BDT uses the following variables: θ_{D^0} , χ^2 of the decay vertex and flight distance of the D^0 candidate, p and p_T of the D^0 candidate and of each of the four final state tracks, χ^2 of the vertex and p_T of the D^{*+} candidate, χ_{IP}^2 of the D^0 candidate and of the final state particles, the maximum distance of closest approach between all pairs of tracks forming the D^0 and D^{*+} candidates, and the p_T and χ_{IP}^2 of the bachelor pion from the D^{*+} candidate.

The BDT discriminant is used to classify each candidate. Assuming a signal branching fraction of 10^{-9} , an optimisation study is performed to choose the combined BDT and muon particle identification (PID) selection criteria that maximise the expected statistical significance of the signal. This significance is defined as $S/\sqrt{S+B}$, where S and B are the signal and background yields respectively. The PID information is quantified as the difference in the log-likelihood of the detector response under different particle mass hypotheses (DLL) [8,20]. The optimisation procedure yields an optimal threshold for the BDT discriminant and a minimum value for $\text{DLL}_{\mu\pi}$ (the difference between the muon and pion hypotheses) of 1.5 for both μ candidates. In addition, the pion candidate is required to have $\text{DLL}_{K\pi}$ less than 3.0 and $\text{DLL}_{p\pi}$ less than 2.0, and each muon candidate must not share hits in the muon stations with any other muon candidate. In the 2% of events in which multiple candidates are reconstructed, the candidate with the smallest D^0 vertex χ^2 is chosen.

The bachelor π^+ of the $D^{*+} \rightarrow D^0\pi^+$ decay is constrained to the PV using a Kalman filter [21]. This constraint improves the resolution for the mass difference between the D^{*+} and the D^0 candidates, $\Delta m \equiv m(\pi^+\pi^-\mu^+\mu^-\pi^+) - m(\pi^+\pi^-\mu^+\mu^-)$, by a factor of two, down to 0.3 MeV/c^2 . Candidates are selected with a Δm value in the range 140.0–151.4 MeV/c^2 .

Candidates from the kinematically similar decay $D^0 \rightarrow \pi^+\pi^-\pi^+\pi^-$ form an important peaking background due to the possible misidentification of two oppositely charged pions as muons. A sample of this hadronic background is retained with a selection that is identical to that applied to the signal except that no muon identification is required. These candidates are then reconstructed under the $D^0 \rightarrow \pi^+\pi^-\mu^+\mu^-$ hypothesis and a subsample of the candidates, in which at least one such pion satisfies the muon identification requirements, is used to determine the shape of this peaking background in each region of dimuon mass, $m(\mu^+\mu^-)$. Under the correct mass hypotheses the $D^0 \rightarrow \pi^+\pi^-\pi^+\pi^-$ candidates are also used as a control sample to check differences between data and simulation that may affect the event selection performance. Moreover, they are used to determine the expected signal shape in each $m(\mu^+\mu^-)$ region by subdividing the $D^0 \rightarrow \pi^+\pi^-\pi^+\pi^-$ sample in the same regions of $m(\pi^+\pi^-)$.

Another potential source of peaking background is due to $\Lambda_c(2595)^+ \rightarrow \Sigma_c(2455)^0\pi^+$ decays, followed by the $\Sigma_c(2455)^0 \rightarrow \Lambda_c^+\pi^-$ and then $\Lambda_c^+ \rightarrow pK^-\pi^+$ decays, with the two pions in the decay chain misidentified as muons and the proton and the kaon misidentified as pions. Therefore, the $\text{DLL}_{K\pi}$ and $\text{DLL}_{p\pi}$ requirements are tightened to be less than zero for the low- $m(\mu^+\mu^-)$

Table 1

$D^0 \rightarrow \pi^+\pi^-\mu^+\mu^-$ fitted yields in the four $m(\mu^+\mu^-)$ regions. The corresponding signal fractions under the assumption of a phase-space model, as described in Section 7, are listed in the last column.

Range description	$m(\mu^+\mu^-)$ [MeV/ c^2]	$D^0 \rightarrow \pi^+\pi^-\mu^+\mu^-$ yield	Fraction
low- $m(\mu^+\mu^-)$	250–525	2 ± 2	30.6%
ρ/ω	565–950	23 ± 6	43.4%
ϕ	950–1100	63 ± 10	10.1%
high- $m(\mu^+\mu^-)$	> 1100	3 ± 2	8.9%

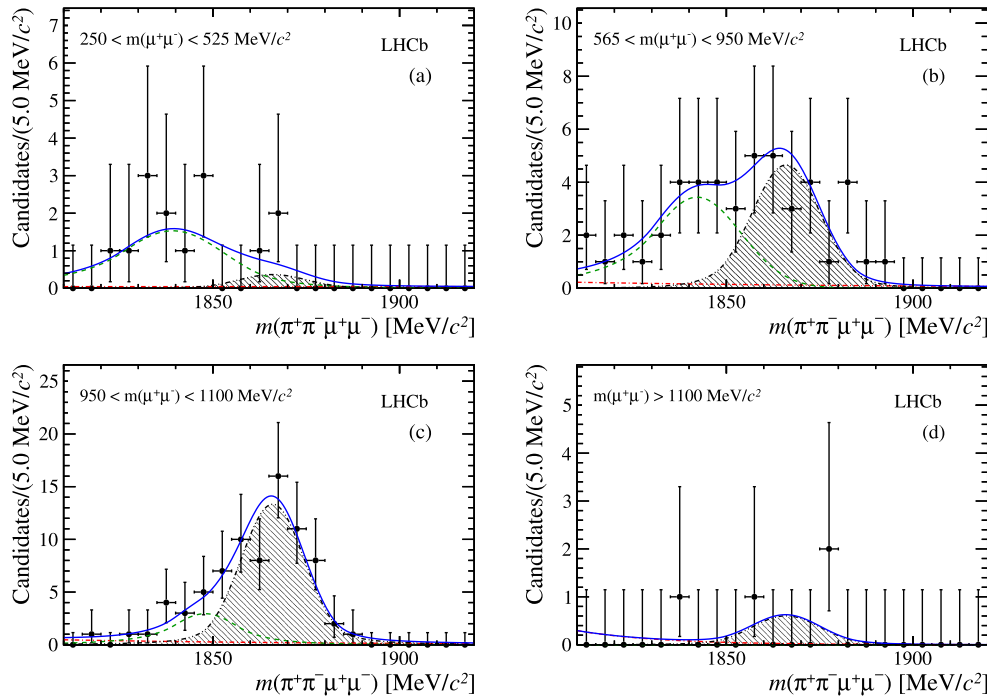


Fig. 2. Distributions of $m(\pi^+\pi^-\mu^+\mu^-)$ for $D^0 \rightarrow \pi^+\pi^-\mu^+\mu^-$ candidates in the (a) low- $m(\mu^+\mu^-)$, (b) ρ/ω , (c) ϕ , and (d) high- $m(\mu^+\mu^-)$ regions, with Δm in the range 144.4–146.6 MeV/ c^2 . The data are shown as points (black) and the fit result (dark blue line) is overlaid. The components of the fit are also shown: the signal (filled area), the $D^0 \rightarrow \pi^+\pi^-\pi^+\pi^-$ background (green dashed line) and the non-peaking background (red dashed-dotted line).

region, where the baryonic background is concentrated, suppressing this background to a negligible level.

Another potentially large background from the $D^0 \rightarrow \pi^+\pi^-\eta$ decay, followed by the decay $\eta \rightarrow \mu^+\mu^-\gamma$, does not peak at the D^0 mass since candidates in which the $m(\mu^+\mu^-)$ is within ± 20 MeV/ c^2 of the nominal η mass are removed from the final fit. The remaining contribution to low values of the $m(\pi^+\pi^-\mu^+\mu^-)$ invariant mass is included in the combinatorial background.

4. Mass fit

The shapes and yields of the signal and background contributions are determined using an unbinned maximum likelihood fit to the two-dimensional $[m(\pi^+\pi^-\mu^+\mu^-), \Delta m]$ distributions in the ranges 1810–1920 and 140–151.4 MeV/ c^2 , respectively. This range is chosen to contain all reconstructed $D^0 \rightarrow \pi^+\pi^-\mu^+\mu^-$ candidates.

The $D^0 \rightarrow \pi^+\pi^-\mu^+\mu^-$ data are split into four regions of $m(\mu^+\mu^-)$: two regions containing the ρ/ω and ϕ resonances and two signal regions, referred to as low- $m(\mu^+\mu^-)$ and high- $m(\mu^+\mu^-)$, respectively. The definitions of these regions are provided in Table 1.

The D^0 mass and Δm shapes for $D^0 \rightarrow \pi^+\pi^-\mu^+\mu^-$ candidates are described by a double Crystal Ball function [22,23], which consists of a Gaussian core and independent left and right power-law tails, on either sides of the core. The parameters of these

shapes are determined from the $D^0 \rightarrow \pi^+\pi^-\pi^+\pi^-$ control sample independently for each of the four $m(\mu^+\mu^-)$ regions.

The $D^0 \rightarrow \pi^+\pi^-\pi^+\pi^-$ peaking background is also split into the predefined dimuon mass regions and is fitted with a double Crystal Ball function. This provides a well-defined shape for this prominent background, which is included in the fit to the signal sample. The yield of the misidentified component is allowed to vary and fitted in each region of the analysis. The combinatorial background is described by an exponential function in the D^0 candidate mass, while the shape in Δm is described by the empirical function $f_{\Delta}(\Delta m, a) = 1 - e^{-(\Delta m - \Delta m_0)/a}$, where the parameter Δm_0 is fixed to 139.6 MeV/ c^2 . The two-dimensional shape used in the fit implicitly assumes that $m(\pi^+\pi^-\mu^+\mu^-)$ and Δm are not correlated.

All the floating coefficients are allowed to vary independently in each of the $m(\mu^+\mu^-)$ regions. Migration between the regions is found to be negligible from simulation studies. The yield observed in the ϕ region is used to normalise the yields in the signal regions.

One-dimensional projections for the D^0 candidate invariant mass and Δm spectra, together with the result of the fits, are shown in Figs. 2 and 3, respectively. The signal yields, which include contributions from the tails of the $m(\mu^+\mu^-)$ resonances leaking into the low- and high- $m(\mu^+\mu^-)$ ranges, are shown in Table 1. No significant excess of candidates is seen in either of the two signal regions.

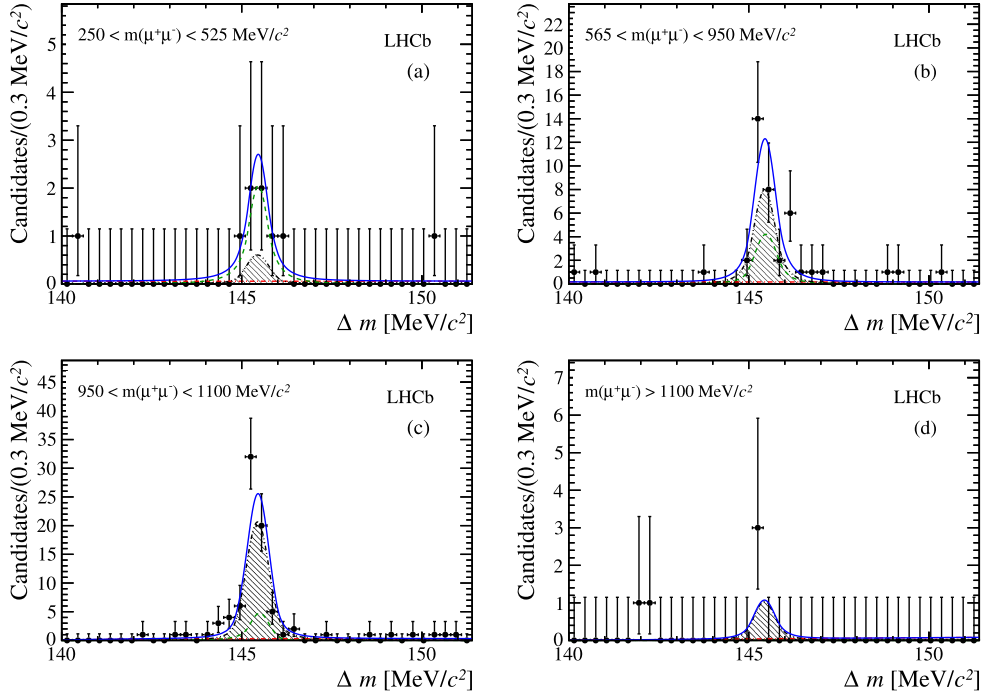


Fig. 3. Distributions of Δm for $D^0 \rightarrow \pi^+\pi^-\mu^+\mu^-$ candidates in the (a) low- $m(\mu^+\mu^-)$, (b) ρ/ω , (c) ϕ , and (d) high- $m(\mu^+\mu^-)$ regions, with the D^0 invariant mass in the range 1840–1888 MeV/c^2 . The data are shown as points (black) and the fit result (dark blue line) is overlaid. The components of the fit are also shown: the signal (filled area), the $D^0 \rightarrow \pi^+\pi^-\pi^+\pi^-$ background (green dashed line) and the non-peaking background (red dashed-dotted line).

The yields in the signal regions are compatible with the expectations from leakage from the $m(\mu^+\mu^-)$ resonant regions. The number of expected events from leakage is calculated assuming the $m(\mu^+\mu^-)$ spectrum given by a sum of relativistic Breit–Wigner functions, describing the η , ρ/ω and ϕ resonances. The contribution from each resonance is scaled according to the branching fractions as determined from resonant $D^0 \rightarrow K^+K^-\pi^+\pi^-$ and $D^0 \rightarrow \pi^+\pi^-\pi^+\pi^-$ decays [24]. The resulting shape is used to extrapolate the yields fitted in the ϕ and ρ regions into the $m(\mu^+\mu^-)$ signal regions. An additional extrapolation is performed using the signal yield in the $m(\mu^+\mu^-)$ range 773–793 MeV/c^2 , where the contribution from the ω resonance is enhanced. In this approach the interference among different resonances is not accounted for and a systematic uncertainty to the extrapolated yield is assigned according to the spread in their extrapolations. The expected number of leakage events is estimated to be 1 ± 1 in both the low- and high- $m(\mu^+\mu^-)$ regions. This precision of this estimate is dominated by the systematic uncertainty.

5. Branching fraction determination

The $D^0 \rightarrow \pi^+\pi^-\mu^+\mu^-$ branching fraction ratio for each $m(\mu^+\mu^-)$ signal region i is calculated using

$$\frac{\mathcal{B}(D^0 \rightarrow \pi^+\pi^-\mu^+\mu^-)^i}{\mathcal{B}(D^0 \rightarrow \pi^+\pi^-\phi(\rightarrow \mu^+\mu^-))} = \frac{N_{D^0 \rightarrow \pi^+\pi^-\mu^+\mu^-}^i}{N_{D^0 \rightarrow \pi^+\pi^-\phi(\rightarrow \mu^+\mu^-)}} \times \frac{\epsilon_{D^0 \rightarrow \pi^+\pi^-\phi(\rightarrow \mu^+\mu^-)}}{\epsilon_{D^0 \rightarrow \pi^+\pi^-\mu^+\mu^-}^i}. \quad (1)$$

The yield and efficiency are given by $N_{D^0 \rightarrow \pi^+\pi^-\mu^+\mu^-}$ and $\epsilon_{D^0 \rightarrow \pi^+\pi^-\mu^+\mu^-}$, respectively, for the signal channel, and by $N_{D^0 \rightarrow \pi^+\pi^-\phi(\rightarrow \mu^+\mu^-)}$ and $\epsilon_{D^0 \rightarrow \pi^+\pi^-\phi(\rightarrow \mu^+\mu^-)}$ for the reference channel. The values for the efficiency ratio $\epsilon_{D^0 \rightarrow \pi^+\pi^-\mu^+\mu^-} / \epsilon_{D^0 \rightarrow \pi^+\pi^-\phi(\rightarrow \mu^+\mu^-)}$ in the low- $m(\mu^+\mu^-)$ and high- $m(\mu^+\mu^-)$ regions, as estimated from simulations, are 0.24 ± 0.03 and

0.69 ± 0.11 , respectively, where the uncertainty reflects the limited statistics of the simulated samples. The efficiencies for reconstructing the signal decay mode and the reference mode include the geometric acceptance of the detector, the efficiencies for track reconstruction, particle identification, selection and trigger. Both efficiency ratios deviate from unity due to differences in the kinematic distributions of the final state particles in the two decays. Moreover, tighter particle identification requirements are responsible for a lower efficiency ratio in the low- $m(\mu^+\mu^-)$ region. The accuracy with which the simulation reproduces the track reconstruction and particle identification is limited. Therefore, the corresponding efficiencies are also studied in data and systematic uncertainties are assigned.

An upper limit on the absolute branching fraction is given using an estimate of the branching fraction of the normalisation mode. The $D^0 \rightarrow \pi^+\pi^-\phi(\rightarrow \mu^+\mu^-)$ branching fraction is estimated using the results of the amplitude analysis of the $D^0 \rightarrow K^+K^-\pi^+\pi^-$ decay performed at CLEO [25]. Only the fit fraction of the decay modes in which the two kaons originate from an intermediate ϕ resonance are considered and the $D^0 \rightarrow \pi^+\pi^-\phi(\rightarrow \mu^+\mu^-)$ branching fraction is calculated by multiplying this fraction by the total $D^0 \rightarrow K^+K^-\pi^+\pi^-$ branching fraction and using the known value of $\mathcal{B}(\phi \rightarrow \mu^+\mu^-)/\mathcal{B}(\phi \rightarrow K^+K^-)$ [24]. There are several interfering contributions to the $D^0 \rightarrow \pi^+\pi^-\phi(\rightarrow K^+K^-)$ amplitude. Considering the interference fractions provided in Ref. [25], the following estimate for the branching fraction is obtained, $\mathcal{B}(D^0 \rightarrow \pi^+\pi^-\phi(\rightarrow \mu^+\mu^-)) = (5.2 \pm 0.6) \times 10^{-7}$. This estimate includes only the statistical uncertainty and refers to the baseline fit model used for the CLEO measurement. Similar estimates for $\mathcal{B}(D^0 \rightarrow \pi^+\pi^-\phi(\rightarrow \mu^+\mu^-))$ are performed using all the alternative models considered in Ref. [25] assuming the interference fractions to be the same as for the baseline model. The spread among the estimates is used to assign a systematic uncertainty of 17% on $\mathcal{B}(D^0 \rightarrow \pi^+\pi^-\phi(\rightarrow \mu^+\mu^-))$. The above procedure to estimate $\mathcal{B}(D^0 \rightarrow \pi^+\pi^-\phi(\rightarrow \mu^+\mu^-))$ is supported by the narrow width of the ϕ resonance resulting in interference effects with other chan-

Table 2
Relative systematic uncertainties averaged over all the $m(\mu^+\mu^-)$ regions for the efficiency ratio.

Source	Uncertainty (%)
Trigger efficiency	5
Hadron identification	4
Reconstruction and selection efficiency	5
Muon identification	1
Finite simulation sample size	12–16
Total	15–18

nels [25] that are negligible compared to the statistical uncertainty. The estimate for $\mathcal{B}(D^0 \rightarrow \pi^+\pi^-\phi(\rightarrow \mu^+\mu^-))$ is $(5.2 \pm 1.1) \times 10^{-7}$, including both statistical and systematic uncertainties, and is used to set an upper limit on the absolute $D^0 \rightarrow \pi^+\pi^-\mu^+\mu^-$ branching fraction.

A possible alternative normalisation, with respect to the ρ/ω dimuon mass region, would be heavily limited by the low statistics available and the relatively high contamination from $D^0 \rightarrow \pi^+\pi^-\pi^+\pi^-$, as can be seen in Fig. 2(b).

6. Systematic uncertainties

Several systematic uncertainties affect the efficiency ratio. Differences in the particle identification between the signal and the normalisation regions are investigated in data. A tag-and-probe technique applied to $b \rightarrow J/\psi X$ decays provides a large sample of muon candidates to determine the muon identification efficiencies [20]. General agreement between simulation and data is found to a level of 1%, which is assigned as a systematic uncertainty.

The particle identification performance for hadrons is investigated by comparing the efficiency in $D^0 \rightarrow \pi^+\pi^-\pi^+\pi^-$ candidates in data and simulation as a function of the $\text{DLL}_{K\pi}$ requirement. The largest discrepancy between data and simulation on the efficiency ratio is found to be 4% and is taken as a systematic uncertainty.

Several quantities, particularly the impact parameter, are known to be imperfectly reproduced in the simulation. Since this may affect the reconstruction and selection efficiency, a systematic uncertainty is estimated by smearing track properties to reproduce the distributions observed in data. The corresponding variation in the efficiency ratio yields an uncertainty of 5%. The BDT description in simulation is checked using background-subtracted $D^0 \rightarrow \pi^+\pi^-\pi^+\pi^-$ candidates where no significant difference is seen. Therefore, no extra systematic uncertainty is assigned.

The systematic uncertainty due to possible mismodelling of the trigger efficiency in the simulation is assigned as follows. The trigger requirements in simulations are varied reproducing the typical changes of trigger configurations that occurred during data taking and an alternate efficiency ratio is calculated in both the $m(\mu^+\mu^-)$ signal regions. The largest difference between the alternate and the baseline efficiency ratio, 5%, is found in the low- $m(\mu^+\mu^-)$ region. This difference is assumed as the overall systematic uncertainty on the trigger efficiency.

The uncertainties on the efficiency ratio due to the finite size of the simulated samples in the low- and high- $m(\mu^+\mu^-)$ regions are 12% and 16% respectively. The production of significantly larger sample of simulated events is impractical due to the low reconstruction and selection efficiencies, particularly in the signal regions. In addition, the statistical uncertainties of the fitted yields in data, listed in Table 1, dominate the total uncertainty. The sources of uncertainty are summarised in Table 2.

According to simulations, biases in the efficiency ratio introduced by varying the relative contribution of $D^0 \rightarrow \rho^0(\rightarrow \pi\pi)\phi(\rightarrow \mu\mu)$ and three-body $D^0 \rightarrow \pi^+\pi^-\phi(\rightarrow \mu^+\mu^-)$

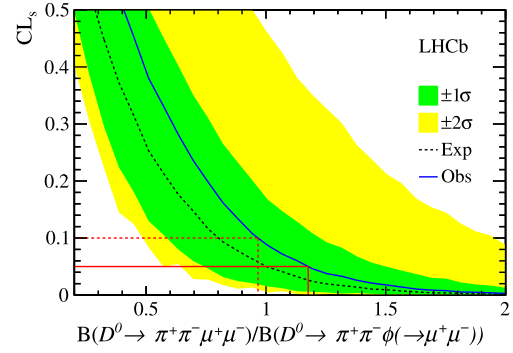


Fig. 4. Observed (solid curve) and expected (dashed curve) CL_s values as a function of $\mathcal{B}(D^0 \rightarrow \pi^+\pi^-\mu^+\mu^-)/\mathcal{B}(D^0 \rightarrow \pi^+\pi^-\phi(\rightarrow \mu^+\mu^-))$. The green (yellow) shaded area contains 68.3% and 95.5% of the results of the analysis on experiments simulated with no signal. The upper limits at the 90(95)% CL are indicated by the dashed (solid) line. (For interpretation of the references to colour in this figure legend, the reader is referred to the web version of this article.)

decays are well within the assigned uncertainty. Varying the value of $\mathcal{B}(D^0 \rightarrow \pi^+\pi^-\phi(\rightarrow \mu^+\mu^-))$ has a negligible effect on the number of leakage events, and no additional systematic uncertainty is assigned.

The systematic uncertainties affecting the yield ratio are taken into account when the branching fraction limits are calculated. The shapes of the signal peaks are taken from the $D^0 \rightarrow \pi^+\pi^-\pi^+\pi^-$ samples separately for each $m(\mu^+\mu^-)$ region to account for variations of the shape as a function of $m(\mu^+\mu^-)$. The impact of alternative shapes for the signal and misidentified $D^0 \rightarrow \pi^+\pi^-\pi^+\pi^-$ decays on the fitted yields and the final limit are investigated. The signal and misidentification background shapes in the signal regions are fitted using the shapes obtained in the ϕ region, and from $D^0 \rightarrow \pi^+\pi^-\pi^+\pi^-$ events reconstructed as $D^0 \rightarrow \pi^+\pi^-\mu^+\mu^-$, but without any muon identification requirements. The change in the result is negligible.

The absolute branching fraction limit includes an extra uncertainty of 21% from the estimate of the branching fraction of the normalisation mode.

7. Results

The compatibility of the observed distribution of candidates with a signal plus background or background-only hypothesis is evaluated using the CL_s method [26,27], which includes the treatment of systematic uncertainties. Upper limits on the non-resonant $D^0 \rightarrow \pi^+\pi^-\mu^+\mu^-$ to $D^0 \rightarrow \pi^+\pi^-\phi(\rightarrow \mu^+\mu^-)$ branching fraction ratio and on the absolute $D^0 \rightarrow \pi^+\pi^-\mu^+\mu^-$ branching fraction are determined using the observed distribution of CL_s as a function of the branching fraction in each $m(\mu^+\mu^-)$ search region. The extrapolation to the full $m(\mu^+\mu^-)$ phase-space is performed assuming a four-body phase-space model for $D^0 \rightarrow \pi^+\pi^-\mu^+\mu^-$ for which fractions in each $m(\mu^+\mu^-)$ region are quoted in Table 1. The observed distribution of CL_s as a function of the total branching fraction ratio for $D^0 \rightarrow \pi^+\pi^-\mu^+\mu^-$ is shown in Fig. 4. A similar distribution for the absolute branching fraction is shown in Fig. 5. The upper limits on the branching fraction ratio and absolute branching fraction at 90% and 95% CL and the p-values $(1 - CL_b)$ for the background-only hypothesis are given in Table 3 and in Table 4. The p-values are computed for the branching fraction value at which CL_{s+b} equals 0.5. Despite the smaller event yield for $D^0 \rightarrow \pi^+\pi^-\mu^+\mu^-$ relative to $D^0 \rightarrow \pi^+\pi^-\phi(\rightarrow \mu^+\mu^-)$, the upper limit on the total relative branching fraction is of order unity due to several factors. These are the low reconstruction and selection efficiency ratio in the signal region, the systematic and

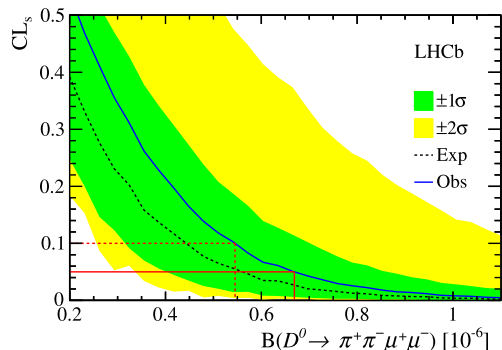


Fig. 5. Observed (solid curve) and expected (dashed curve) CL_s values as a function of $\mathcal{B}(D^0 \rightarrow \pi^+\pi^-\mu^+\mu^-)$. The green (yellow) shaded area contains 68.3% and 95.5% of the results of the analysis on experiments simulated with no signal. The upper limits at the 90(95)% CL are indicated by the dashed (solid) line. (For interpretation of the references to colour in this figure legend, the reader is referred to the web version of this article.)

Table 3

Upper limits on $\mathcal{B}(D^0 \rightarrow \pi^+\pi^-\mu^+\mu^-)/\mathcal{B}(D^0 \rightarrow \pi^+\pi^-\phi(\rightarrow \mu^+\mu^-))$ at 90 and 95% CL, and p-values for the background-only hypothesis in each $m(\mu^+\mu^-)$ region and in the full $m(\mu^+\mu^-)$ range (assuming a phase-space model).

Region	90%	95%	p-value
low- $m(\mu^+\mu^-)$	0.41	0.51	0.32
high- $m(\mu^+\mu^-)$	0.17	0.21	0.12
Total	0.96	1.19	0.25

Table 4

Upper limits on $\mathcal{B}(D^0 \rightarrow \pi^+\pi^-\mu^+\mu^-)$ at 90 and 95% CL in each $m(\mu^+\mu^-)$ region and in the full $m(\mu^+\mu^-)$ range (assuming a phase-space model).

Region	90% [$\times 10^{-7}$]	95% [$\times 10^{-7}$]
low- $m(\mu^+\mu^-)$	2.3	2.9
high- $m(\mu^+\mu^-)$	1.0	1.2
Total	5.5	6.7

statistical uncertainties, and the extrapolation to the full $m(\mu^+\mu^-)$ range according to a phase-space model.

It is noted that, while the results in individual $m(\mu^+\mu^-)$ regions naturally include possible contributions from $D^0 \rightarrow \rho(\rightarrow \pi^+\pi^-)\mu^+\mu^-$ since differences in the reconstruction and selection efficiency with respect to the four-body $D^0 \rightarrow \pi^+\pi^-\mu^+\mu^-$ are negligible, the extrapolation to the full $m(\mu^+\mu^-)$ phase-space depends on the four-body assumption. Distinguishing a ρ component in the dipion mass spectrum requires an amplitude analysis which would be hardly informative given the small sample size and beyond the scope of this first search.

Contributions for non-resonant $D^0 \rightarrow \pi^+\pi^-\mu^+\mu^-$ events in the normalisation mode $m(\mu^+\mu^-)$ window are neglected in the upper limit calculations. Assuming a branching fraction equal to the 90% CL upper limit set in the highest $m(\mu^+\mu^-)$ region, the relative contribution of the non-resonant mode is estimated to be less than 3%, which is small compared with other uncertainties.

8. Conclusions

A search for the $D^0 \rightarrow \pi^+\pi^-\mu^+\mu^-$ decay is conducted using pp collision data, corresponding to an integrated luminosity of 1.0 fb^{-1} at $\sqrt{s} = 7 \text{ TeV}$ recorded by the LHCb experiment. The numbers of events in the non-resonant $m(\mu^+\mu^-)$ regions are compatible with the background-only hypothesis. The limits set on branching fractions in two $m(\mu^+\mu^-)$ bins and on the total branching fraction, excluding the resonant contributions and assuming a phase-space model, are

$$\frac{\mathcal{B}(D^0 \rightarrow \pi^+\pi^-\mu^+\mu^-)}{\mathcal{B}(D^0 \rightarrow \pi^+\pi^-\phi(\rightarrow \mu^+\mu^-))} < 0.96(1.19),$$

at the 90(95)% CL,

$$\mathcal{B}(D^0 \rightarrow \pi^+\pi^-\mu^+\mu^-) < 5.5(6.7) \times 10^{-7},$$

at the 90(95)% CL.

The upper limit on the absolute branching fraction is improved by a factor of 50 with respect to the previous search [5], yielding the most stringent result to date.

Acknowledgements

We express our gratitude to our colleagues in the CERN accelerator departments for the excellent performance of the LHC. We thank the technical and administrative staff at the LHCb institutes. We acknowledge support from CERN and from the national agencies: CAPES, CNPq, FAPERJ and FINEP (Brazil); NSFC (China); CNRS/IN2P3 and Region Auvergne (France); BMBF, DFG, HGF and MPG (Germany); SFI (Ireland); INFN (Italy); FOM and NWO (The Netherlands); SCSR (Poland); MEN/IFA (Romania); MinES, Rosatom, RFBR and NRC ‘‘Kurchatov Institute’’ (Russia); MinEco, XuntaGal and GENCAT (Spain); SNSF and SER (Switzerland); NAS Ukraine (Ukraine); STFC (United Kingdom); NSF (USA). We also acknowledge the support received from the ERC under FP7. The Tier1 computing centres are supported by IN2P3 (France), KIT and BMBF (Germany), INFN (Italy), NWO and SURF (The Netherlands), PIC (Spain), GridPP (United Kingdom). We are thankful for the computing resources put at our disposal by Yandex LLC (Russia), as well as to the communities behind the multiple open source software packages that we depend on.

References

- [1] S. Fajfer, S. Prelovsek, Search for new physics in rare D decays, in: ICHEP 2006, Conf. Proc. C060726 (2006) 811, arXiv:hep-ph/0610032.
- [2] S. Fajfer, N. Kosnik, S. Prelovsek, Updated constraints on new physics in rare charm decays, Phys. Rev. D 76 (2007) 074010, arXiv:0706.1133.
- [3] A. Paul, I.I. Bigi, S. Recksiegel, On $D \rightarrow X_{u,l} l^+ l^-$ within the Standard Model and frameworks like the littlest Higgs model with T parity, Phys. Rev. D 83 (2011) 114006, arXiv:1101.6053.
- [4] L. Cappiello, O. Cata, G. D’Ambrosio, Standard Model prediction and new physics tests for $D^0 \rightarrow h_1^+ h_2^- l^+ l^-$ ($h = \pi, K; l = e, \mu$), J. High Energy Phys. 1304 (2013) 135, arXiv:1209.4235.
- [5] E791 Collaboration, E. Aitala, et al., Search for rare and forbidden charm meson decays $D^0 \rightarrow V l^+ l^-$ and $h h l l$, Phys. Rev. Lett. 86 (2001) 3969, arXiv:hep-ex/0011077.
- [6] LHCb Collaboration, R. Aaij, et al., Search for $D_{(s)}^+ \rightarrow \pi^+ \mu^+ \mu^-$ and $D_{(s)}^+ \rightarrow \pi^- \mu^+ \mu^+$ decays, Phys. Lett. B 724 (2013) 203, arXiv:1304.6365.
- [7] LHCb Collaboration, A.A. Alves Jr., et al., The LHCb detector at the LHC, J. Instrum. 3 (2008) S08005.
- [8] M. Adinolfi, et al., Performance of the LHCb RICH detector at the LHC, Eur. Phys. J. C 73 (2013) 2431, arXiv:1211.6759.
- [9] A.A. Alves Jr., et al., Performance of the LHCb muon system, J. Instrum. 8 (2013) P02022, arXiv:1211.1346.
- [10] R. Aaij, et al., The LHCb trigger and its performance in 2011, J. Instrum. 8 (2013) P04022, arXiv:1211.3055.
- [11] T. Sjöstrand, S. Mrenna, P. Skands, PYTHIA 6.4 physics and manual, J. High Energy Phys. 0605 (2006) 026, arXiv:hep-ph/0603175.
- [12] I. Belyaev, et al., Handling of the generation of primary events in GAUSS, the LHCb simulation framework, in: Nuclear Science Symposium Conference Record, NSS/MIC, IEEE, 2010, p. 1155.
- [13] D.J. Lange, The EvtGen particle decay simulation package, Nucl. Instrum. Methods, Sect. A 462 (2001) 152.
- [14] Geant4 Collaboration, J. Allison, et al., Geant4 developments and applications, IEEE Trans. Nucl. Sci. 53 (2006) 270.
- [15] Geant4 Collaboration, S. Agostinelli, et al., Geant4: a simulation toolkit, Nucl. Instrum. Methods, Sect. A 506 (2003) 250.
- [16] M. Clemencic, et al., The LHCb simulation application, GAUSS: design, evolution and experience, J. Phys. Conf. Ser. 331 (2011) 032023.
- [17] L. Breiman, J.H. Friedman, R.A. Olshen, C.J. Stone, Classification and Regression Trees, Wadsworth International Group, Belmont, California, USA, 1984.

- [18] B.P. Roe, et al., Boosted decision trees as an alternative to artificial neural networks for particle identification, Nucl. Instrum. Methods, Sect. A 543 (2005) 577, arXiv:physics/0408124.
- [19] A. Hoecker, et al., TMVA: Toolkit for multivariate data analysis, PoS ACAT (2007) 040, arXiv:physics/0703039.
- [20] F. Archilli, et al., Performance of the muon identification at LHCb, JINST, <http://dx.doi.org/10.1088/1748-0221/8/10/P10020>, arXiv:1306.0249.
- [21] W.D. Hulsbergen, Decay chain fitting with a Kalman filter, Nucl. Instrum. Methods, Sect. A 552 (2005) 566, arXiv:physics/0503191.
- [22] J. Gaiser, Charmonium spectroscopy from radiative decays of the J/ψ and ψ' , PhD thesis, Calif. Univ. Stanford, 1982, SLAC-0255, UMI-83-14449-MC, SLAC-R-0255, SLAC-R-255.
- [23] T. Skwarnicki, A study of the radiative cascade transitions between the Υ' and Υ resonances, PhD thesis, Institute of Nuclear Physics, Krakow, 1986, DESY-F31-86-02.
- [24] Particle Data Group, J. Beringer, et al., Review of particle physics, Phys. Rev. D 86 (2012) 010001, and 2013 partial update for the 2014 edition.
- [25] CLEO Collaboration, M. Artuso, et al., Amplitude analysis of $D^0 \rightarrow K^+ K^- \pi^+ \pi^-$, Phys. Rev. D 85 (2012) 122002, arXiv:1201.5716.
- [26] A.L. Read, Presentation of search results: the CL_s technique, J. Phys. G 28 (2002) 2693.
- [27] T. Junk, Confidence level computation for combining searches with small statistics, Nucl. Instrum. Methods, Sect. A 434 (1999) 435, arXiv:hep-ex/9902006.

LHCb Collaboration

R. Aaij⁴⁰, B. Adeva³⁶, M. Adinolfi⁴⁵, C. Adrover⁶, A. Affolder⁵¹, Z. Ajaltouni⁵, J. Albrecht⁹, F. Alessio³⁷, M. Alexander⁵⁰, S. Ali⁴⁰, G. Alkhazov²⁹, P. Alvarez Cartelle³⁶, A.A. Alves Jr²⁴, S. Amato², S. Amerio²¹, Y. Amhis⁷, L. Anderlini^{17,f}, J. Anderson³⁹, R. Andreassen⁵⁶, J.E. Andrews⁵⁷, R.B. Appleby⁵³, O. Aquines Gutierrez¹⁰, F. Archilli¹⁸, A. Artamonov³⁴, M. Artuso⁵⁸, E. Aslanides⁶, G. Auriemma^{24,m}, M. Baalouch⁵, S. Bachmann¹¹, J.J. Back⁴⁷, A. Badalov³⁵, C. Baesso^{59,t}, V. Balagura³⁰, W. Baldini¹⁶, R.J. Barlow⁵³, C. Barschel³⁷, S. Barsuk⁷, W. Barter⁴⁶, Th. Bauer⁴⁰, A. Bay³⁸, J. Beddow⁵⁰, F. Bedeschi²², I. Bediaga¹, S. Belogurov³⁰, K. Belous³⁴, I. Belyaev³⁰, E. Ben-Haim⁸, G. Bencivenni¹⁸, S. Benson⁴⁹, J. Benton⁴⁵, A. Berezhnoy³¹, R. Bernet³⁹, M.-O. Bettler⁴⁶, M. van Beuzekom⁴⁰, A. Bien¹¹, S. Bifani⁴⁴, T. Bird⁵³, A. Bizzeti^{17,h}, P.M. Bjørnstad⁵³, T. Blake³⁷, F. Blanc³⁸, J. Blouw¹⁰, S. Blusk⁵⁸, V. Bocci²⁴, A. Bondar³³, N. Bondar²⁹, W. Bonivento¹⁵, S. Borghi⁵³, A. Borgia⁵⁸, T.J.V. Bowcock⁵¹, E. Bowen³⁹, C. Bozzi¹⁶, T. Brambach⁹, J. van den Brand⁴¹, J. Bressieux³⁸, D. Brett⁵³, M. Britsch¹⁰, T. Britton⁵⁸, N.H. Brook⁴⁵, H. Brown⁵¹, A. Bursche³⁹, G. Busetto^{21,q}, J. Buytaert³⁷, S. Cadeddu¹⁵, O. Callot⁷, M. Calvi^{20,j}, M. Calvo Gomez^{35,n}, A. Camboni³⁵, P. Campana^{18,37}, D. Campora Perez³⁷, A. Carbone^{14,c}, G. Carboni^{23,k}, R. Cardinale^{19,i}, A. Cardini¹⁵, H. Carranza-Mejia⁴⁹, L. Carson⁵², K. Carvalho Akiba², G. Casse⁵¹, L. Castillo Garcia³⁷, M. Cattaneo³⁷, Ch. Cauet⁹, R. Cenci⁵⁷, M. Charles⁵⁴, Ph. Charpentier³⁷, S.-F. Cheung⁵⁴, N. Chiapolini³⁹, M. Chrzaszcz^{39,25}, K. Ciba³⁷, X. Cid Vidal³⁷, G. Ciezarek⁵², P.E.L. Clarke⁴⁹, M. Clemencic³⁷, H.V. Cliff⁴⁶, J. Closier³⁷, C. Coca²⁸, V. Coco⁴⁰, J. Cogan⁶, E. Cogneras⁵, P. Collins³⁷, A. Comerma-Montells³⁵, A. Contu^{15,37,*}, A. Cook⁴⁵, M. Coombes⁴⁵, S. Coquereau⁸, G. Corti³⁷, B. Couturier³⁷, G.A. Cowan⁴⁹, D.C. Craik⁴⁷, M. Cruz Torres^{59,t}, S. Cunliffe⁵², R. Currie⁴⁹, C. D'Ambrosio³⁷, P. David⁸, P.N.Y. David⁴⁰, A. Davis⁵⁶, I. De Bonis⁴, K. De Bruyn⁴⁰, S. De Capua⁵³, M. De Cian¹¹, J.M. De Miranda¹, L. De Paula², W. De Silva⁵⁶, P. De Simone¹⁸, D. Decamp⁴, M. Deckenhoff⁹, L. Del Buono⁸, N. Déléage⁴, D. Derkach⁵⁴, O. Deschamps⁵, F. Dettori⁴¹, A. Di Canto¹¹, H. Dijkstra³⁷, M. Dogaru²⁸, S. Donleavy⁵¹, F. Dordei¹¹, A. Dosil Suárez³⁶, D. Dossett⁴⁷, A. Dovbnya⁴², F. Dupertuis³⁸, P. Durante³⁷, R. Dzhelyadin³⁴, A. Dziurda²⁵, A. Dzyuba²⁹, S. Easo⁴⁸, U. Egede⁵², V. Egorychev³⁰, S. Eidelman³³, D. van Eijk⁴⁰, S. Eisenhardt⁴⁹, U. Eitschberger⁹, R. Ekelhof⁹, L. Eklund^{50,37}, I. El Rifai⁵, Ch. Elsasser³⁹, A. Falabella^{14,e}, C. Färber¹¹, C. Farinelli⁴⁰, S. Farry⁵¹, D. Ferguson⁴⁹, V. Fernandez Albor³⁶, F. Ferreira Rodrigues¹, M. Ferro-Luzzi³⁷, S. Filippov³², M. Fiore^{16,e}, C. Fitzpatrick³⁷, M. Fontana¹⁰, F. Fontanelli^{19,i}, R. Forty³⁷, O. Francisco², M. Frank³⁷, C. Frei³⁷, M. Frosini^{17,37,f}, E. Furfaro^{23,k}, A. Gallas Torreira³⁶, D. Galli^{14,c}, M. Gandelman², P. Gandini⁵⁸, Y. Gao³, J. Garofoli⁵⁸, P. Garosi⁵³, J. Garra Tico⁴⁶, L. Garrido³⁵, C. Gaspar³⁷, R. Gauld⁵⁴, E. Gersabeck¹¹, M. Gersabeck⁵³, T. Gershon⁴⁷, Ph. Ghez⁴, V. Gibson⁴⁶, L. Giubega²⁸, V.V. Gligorov³⁷, C. Göbel^{59,t}, D. Golubkov³⁰, A. Golutvin^{52,30,37}, A. Gomes², P. Gorbounov^{30,37}, H. Gordon³⁷, M. Grabalosa Gándara⁵, R. Graciani Diaz³⁵, L.A. Granado Cardoso³⁷, E. Graugés³⁵, G. Graziani¹⁷, A. Greco²⁸, E. Greening⁵⁴, S. Gregson⁴⁶, P. Griffith⁴⁴, L. Grillo¹¹, O. Grünberg^{60,u}, B. Gui⁵⁸, E. Gushchin³², Yu. Guz^{34,37}, T. Gys³⁷, C. Hadjivasiliou⁵⁸, G. Haefeli³⁸, C. Haen³⁷, S.C. Haines⁴⁶, S. Hall⁵², B. Hamilton⁵⁷, T. Hampson⁴⁵, S. Hansmann-Menzemer¹¹, N. Harnew⁵⁴, S.T. Harnew⁴⁵, J. Harrison⁵³, T. Hartmann^{60,u}, J. He³⁷, T. Head³⁷, V. Heijne⁴⁰, K. Hennessy⁵¹, P. Henrard⁵, J.A. Hernando Morata³⁶, E. van Herwijnen³⁷, M. Heß^{60,u}, A. Hicheur¹, E. Hicks⁵¹, D. Hill⁵⁴, M. Hoballah⁵, C. Hombach⁵³, W. Hulsbergen⁴⁰, P. Hunt⁵⁴, T. Huse⁵¹, N. Hussain⁵⁴, D. Hutchcroft⁵¹, D. Hynds⁵⁰, V. Iakovenko⁴³, M. Idzik²⁶, P. Ilten¹², R. Jacobsson³⁷, A. Jaeger¹¹, E. Jans⁴⁰, P. Jaton³⁸, A. Jawahery⁵⁷, F. Jing³, M. John⁵⁴, D. Johnson⁵⁴, C.R. Jones⁴⁶, C. Joram³⁷, B. Jost³⁷, M. Kabbalo⁹, S. Kandybei⁴², W. Kanso⁶, M. Karacson³⁷,

T.M. Karbach³⁷, I.R. Kenyon⁴⁴, T. Ketel⁴¹, B. Khanji²⁰, O. Kochebina⁷, I. Komarov³⁸, R.F. Koopman⁴¹, P. Koppenburg⁴⁰, M. Korolev³¹, A. Kozlinskiy⁴⁰, L. Kravchuk³², K. Kreplin¹¹, M. Kreps⁴⁷, G. Krocker¹¹, P. Krokovny³³, F. Kruse⁹, M. Kucharczyk^{20,25,37,j}, V. Kudryavtsev³³, K. Kurek²⁷, T. Kvaratskheliya^{30,37}, V.N. La Thi³⁸, D. Lacarrere³⁷, G. Lafferty⁵³, A. Lai¹⁵, D. Lambert⁴⁹, R.W. Lambert⁴¹, E. Lanciotti³⁷, G. Lanfranchi¹⁸, C. Langenbruch³⁷, T. Latham⁴⁷, C. Lazzeroni⁴⁴, R. Le Gac⁶, J. van Leerdam⁴⁰, J.-P. Lees⁴, R. Lefèvre⁵, A. Leflat³¹, J. Lefrançois⁷, S. Leo²², O. Leroy⁶, T. Lesiak²⁵, B. Leverington¹¹, Y. Li³, L. Li Gioi⁵, M. Liles⁵¹, R. Lindner³⁷, C. Linn¹¹, B. Liu³, G. Liu³⁷, S. Lohn³⁷, I. Longstaff⁵⁰, J.H. Lopes², N. Lopez-March³⁸, H. Lu³, D. Lucchesi^{21,q}, J. Luisier³⁸, H. Luo⁴⁹, O. Lupton⁵⁴, F. Machefert⁷, I.V. Machikhiliyan³⁰, F. Maciuc²⁸, O. Maev^{29,37}, S. Malde⁵⁴, G. Manca^{15,d}, G. Mancinelli⁶, J. Maratas⁵, U. Marconi¹⁴, P. Marino^{22,s}, R. Märki³⁸, J. Marks¹¹, G. Martellotti²⁴, A. Martens⁸, A. Martín Sánchez⁷, M. Martinelli⁴⁰, D. Martinez Santos^{41,37}, D. Martins Tostes², A. Martynov³¹, A. Massafferri¹, R. Matev³⁷, Z. Mathe³⁷, C. Matteuzzi²⁰, E. Maurice⁶, A. Mazurov^{16,37,e}, J. McCarthy⁴⁴, A. McNab⁵³, R. McNulty¹², B. McSkelly⁵¹, B. Meadows^{56,54}, F. Meier⁹, M. Meissner¹¹, M. Merk⁴⁰, D.A. Milanes⁸, M.-N. Minard⁴, J. Molina Rodriguez^{59,t}, S. Monteil⁵, D. Moran⁵³, P. Morawski²⁵, A. Mordà⁶, M.J. Morello^{22,s}, R. Mountain⁵⁸, I. Mous⁴⁰, F. Muheim⁴⁹, K. Müller³⁹, R. Muresan²⁸, B. Muryn²⁶, B. Muster³⁸, P. Naik⁴⁵, T. Nakada³⁸, R. Nandakumar⁴⁸, I. Nasteva¹, M. Needham⁴⁹, S. Neubert³⁷, N. Neufeld³⁷, A.D. Nguyen³⁸, T.D. Nguyen³⁸, C. Nguyen-Mau^{38,o}, M. Nicol⁷, V. Niess⁵, R. Niet⁹, N. Nikitin³¹, T. Nikodem¹¹, A. Nomerotski⁵⁴, A. Novoselov³⁴, A. Oblakowska-Mucha²⁶, V. Obraztsov³⁴, S. Oggero⁴⁰, S. Ogilvy⁵⁰, O. Okhrimenko⁴³, R. Oldeman^{15,d}, M. Orlandea²⁸, J.M. Otalora Goicochea², P. Owen⁵², A. Oyanguren³⁵, B.K. Pal⁵⁸, A. Palano^{13,b}, M. Palutan¹⁸, J. Panman³⁷, A. Papanestis⁴⁸, M. Pappagallo⁵⁰, C. Parkes⁵³, C.J. Parkinson⁵², G. Passaleva¹⁷, G.D. Patel⁵¹, M. Patel⁵², G.N. Patrick⁴⁸, C. Patrignani^{19,i}, C. Pavel-Nicorescu²⁸, A. Pazos Alvarez³⁶, A. Pearce⁵³, A. Pellegrino⁴⁰, G. Penso^{24,l}, M. Pepe Altarelli³⁷, S. Perazzini^{14,c}, E. Perez Trigo³⁶, A. Pérez-Calero Yzquierdo³⁵, P. Perret⁵, M. Perrin-Terrin⁶, L. Pescatore⁴⁴, E. Pesen^{61,v}, G. Pessina²⁰, K. Petridis⁵², A. Petrolini^{19,i}, A. Phan⁵⁸, E. Picatoste Olloqui³⁵, B. Pietrzyk⁴, T. Pilař⁴⁷, D. Pinci²⁴, S. Playfer⁴⁹, M. Plo Casasus³⁶, F. Polci⁸, G. Polok²⁵, A. Poluektov^{47,33}, E. Polcarpo², A. Popov³⁴, D. Popov¹⁰, B. Popovici²⁸, C. Potterat³⁵, A. Powell⁵⁴, J. Prisciandaro³⁸, A. Pritchard⁵¹, C. Prouve⁷, V. Pugatch⁴³, A. Puig Navarro³⁸, G. Punzi^{22,r}, W. Qian⁴, B. Rachwal²⁵, J.H. Rademacker⁴⁵, B. Rakotomiaramanana³⁸, M.S. Rangel², I. Raniuk⁴², N. Rauschmayr³⁷, G. Raven⁴¹, S. Redford⁵⁴, S. Reichert⁵³, M.M. Reid⁴⁷, A.C. dos Reis¹, S. Ricciardi⁴⁸, A. Richards⁵², K. Rinnert⁵¹, V. Rives Molina³⁵, D.A. Roa Romero⁵, P. Robbe⁷, D.A. Roberts⁵⁷, A.B. Rodrigues¹, E. Rodrigues⁵³, P. Rodriguez Perez³⁶, S. Roiser³⁷, V. Romanovsky³⁴, A. Romero Vidal³⁶, M. Rotondo²¹, J. Rouvinet³⁸, T. Ruf³⁷, F. Ruffini²², H. Ruiz³⁵, P. Ruiz Valls³⁵, G. Sabatino^{24,k}, J.J. Saborido Silva³⁶, N. Sagidova²⁹, P. Sail⁵⁰, B. Saitta^{15,d}, V. Salustino Guimaraes², B. Sanmartin Sedes³⁶, R. Santacesaria²⁴, C. Santamarina Rios³⁶, E. Santovetti^{23,k}, M. Sapunov⁶, A. Sarti¹⁸, C. Satriano^{24,m}, A. Satta²³, M. Savrie^{16,e}, D. Savrina^{30,31}, M. Schiller⁴¹, H. Schindler³⁷, M. Schlupp⁹, M. Schmelling¹⁰, B. Schmidt³⁷, O. Schneider³⁸, A. Schopper³⁷, M.-H. Schune⁷, R. Schwemmer³⁷, B. Sciascia¹⁸, A. Sciubba²⁴, M. Seco³⁶, A. Semennikov³⁰, K. Senderowska²⁶, I. Sepp⁵², N. Serra³⁹, J. Serrano⁶, P. Seyfert¹¹, M. Shapkin³⁴, I. Shapoval^{16,42,e}, Y. Shcheglov²⁹, T. Shears⁵¹, L. Shekhtman³³, O. Shevchenko⁴², V. Shevchenko³⁰, A. Shires⁹, R. Silva Coutinho⁴⁷, M. Sirendi⁴⁶, N. Skidmore⁴⁵, T. Skwarnicki⁵⁸, N.A. Smith⁵¹, E. Smith^{54,48}, E. Smith⁵², J. Smith⁴⁶, M. Smith⁵³, M.D. Sokoloff⁵⁶, F.J.P. Soler⁵⁰, F. Soomro³⁸, D. Souza⁴⁵, B. Souza De Paula², B. Spaan⁹, A. Sparkes⁴⁹, P. Spradlin⁵⁰, F. Stagni³⁷, S. Stahl¹¹, O. Steinkamp³⁹, S. Stevenson⁵⁴, S. Stoica²⁸, S. Stone⁵⁸, B. Storaci³⁹, M. Straticiuc²⁸, U. Straumann³⁹, V.K. Subbiah³⁷, L. Sun⁵⁶, W. Sutcliffe⁵², S. Swientek⁹, V. Syropoulos⁴¹, M. Szczekowski²⁷, P. Szczypka^{38,37}, D. Szilard², T. Szumlak²⁶, S. T'Jampens⁴, M. Teklishyn⁷, E. Teodorescu²⁸, F. Teubert³⁷, C. Thomas⁵⁴, E. Thomas³⁷, J. van Tilburg¹¹, V. Tisserand⁴, M. Tobin³⁸, S. Tolk⁴¹, D. Tonelli³⁷, S. Topp-Joergensen⁵⁴, N. Torr⁵⁴, E. Tournefier^{4,52}, S. Tourneur³⁸, M.T. Tran³⁸, M. Tresch³⁹, A. Tsaregorodtsev⁶, P. Tsopelas⁴⁰, N. Tuning^{40,37}, M. Ubeda Garcia³⁷, A. Ukleja²⁷, A. Ustyuzhanin^{52,p}, U. Uwer¹¹, V. Vagnoni¹⁴, G. Valenti¹⁴, A. Vallier⁷, R. Vazquez Gomez¹⁸, P. Vazquez Regueiro³⁶, C. Vázquez Sierra³⁶, S. Vecchi¹⁶, J.J. Velthuis⁴⁵, M. Veltri^{17,g}, G. Veneziano³⁸, M. Vesterinen³⁷, B. Viaud⁷, D. Vieira², X. Vilasis-Cardona^{35,n}, A. Vollhardt³⁹, D. Volyanskyy¹⁰, D. Voong⁴⁵, A. Vorobyev²⁹, V. Vorobyev³³, C. Voß^{60,u}, H. Voss¹⁰, R. Waldi^{60,u}, C. Wallace⁴⁷, R. Wallace¹², S. Wandernoth¹¹, J. Wang⁵⁸, D.R. Ward⁴⁶, N.K. Watson⁴⁴, A.D. Webber⁵³, D. Websdale⁵²,

M. Whitehead⁴⁷, J. Wicht³⁷, J. Wiechczynski²⁵, D. Wiedner¹¹, L. Wiggers⁴⁰, G. Wilkinson⁵⁴,
 M.P. Williams^{47,48}, M. Williams⁵⁵, F.F. Wilson⁴⁸, J. Wimberley⁵⁷, J. Wishahi⁹, W. Wislicki²⁷,
 M. Witek²⁵, G. Wormser⁷, S.A. Wotton⁴⁶, S. Wright⁴⁶, S. Wu³, K. Wyllie³⁷, Y. Xie^{49,37}, Z. Xing⁵⁸,
 Z. Yang³, X. Yuan³, O. Yushchenko³⁴, M. Zangoli¹⁴, M. Zavertyaev^{10,a}, F. Zhang³, L. Zhang⁵⁸,
 W.C. Zhang¹², Y. Zhang³, A. Zhelezov¹¹, A. Zhokhov³⁰, L. Zhong³, A. Zvyagin³⁷

¹ Centro Brasileiro de Pesquisas Físicas (CBPF), Rio de Janeiro, Brazil

² Universidade Federal do Rio de Janeiro (UFRJ), Rio de Janeiro, Brazil

³ Center for High Energy Physics, Tsinghua University, Beijing, China

⁴ LAPP, Université de Savoie, CNRS/IN2P3, Annecy-Le-Vieux, France

⁵ Clermont Université, Université Blaise Pascal, CNRS/IN2P3, LPC, Clermont-Ferrand, France

⁶ CPPM, Aix-Marseille Université, CNRS/IN2P3, Marseille, France

⁷ LAL, Université Paris-Sud, CNRS/IN2P3, Orsay, France

⁸ LPNHE, Université Pierre et Marie Curie, Université Paris Diderot, CNRS/IN2P3, Paris, France

⁹ Fakultät Physik, Technische Universität Dortmund, Dortmund, Germany

¹⁰ Max-Planck-Institut für Kernphysik (MPIK), Heidelberg, Germany

¹¹ Physikalisches Institut, Ruprecht-Karls-Universität Heidelberg, Heidelberg, Germany

¹² School of Physics, University College Dublin, Dublin, Ireland

¹³ Sezione INFN di Bari, Bari, Italy

¹⁴ Sezione INFN di Bologna, Bologna, Italy

¹⁵ Sezione INFN di Cagliari, Cagliari, Italy

¹⁶ Sezione INFN di Ferrara, Ferrara, Italy

¹⁷ Sezione INFN di Firenze, Firenze, Italy

¹⁸ Laboratori Nazionali dell'INFN di Frascati, Frascati, Italy

¹⁹ Sezione INFN di Genova, Genova, Italy

²⁰ Sezione INFN di Milano Bicocca, Milano, Italy

²¹ Sezione INFN di Padova, Padova, Italy

²² Sezione INFN di Pisa, Pisa, Italy

²³ Sezione INFN di Roma Tor Vergata, Roma, Italy

²⁴ Sezione INFN di Roma La Sapienza, Roma, Italy

²⁵ Henryk Niewodniczanski Institute of Nuclear Physics Polish Academy of Sciences, Kraków, Poland

²⁶ AGH – University of Science and Technology, Faculty of Physics and Applied Computer Science, Kraków, Poland

²⁷ National Center for Nuclear Research (NCBJ), Warsaw, Poland

²⁸ Horia Hulubei National Institute of Physics and Nuclear Engineering, Bucharest-Magurele, Romania

²⁹ Petersburg Nuclear Physics Institute (PNPI), Gatchina, Russia

³⁰ Institute of Theoretical and Experimental Physics (ITEP), Moscow, Russia

³¹ Institute of Nuclear Physics, Moscow State University (SINP MSU), Moscow, Russia

³² Institute for Nuclear Research of the Russian Academy of Sciences (INR RAN), Moscow, Russia

³³ Budker Institute of Nuclear Physics (SB RAS) and Novosibirsk State University, Novosibirsk, Russia

³⁴ Institute for High Energy Physics (IHEP), Protvino, Russia

³⁵ Universitat de Barcelona, Barcelona, Spain

³⁶ Universidad de Santiago de Compostela, Santiago de Compostela, Spain

³⁷ European Organization for Nuclear Research (CERN), Geneva, Switzerland

³⁸ Ecole Polytechnique Fédérale de Lausanne (EPFL), Lausanne, Switzerland

³⁹ Physik-Institut, Universität Zürich, Zürich, Switzerland

⁴⁰ Nikhef National Institute for Subatomic Physics, Amsterdam, The Netherlands

⁴¹ Nikhef National Institute for Subatomic Physics and VU University Amsterdam, Amsterdam, The Netherlands

⁴² NSC Kharkiv Institute of Physics and Technology (NSC KIPT), Kharkiv, Ukraine

⁴³ Institute for Nuclear Research of the National Academy of Sciences (KINR), Kyiv, Ukraine

⁴⁴ University of Birmingham, Birmingham, United Kingdom

⁴⁵ H.H. Wills Physics Laboratory, University of Bristol, Bristol, United Kingdom

⁴⁶ Cavendish Laboratory, University of Cambridge, Cambridge, United Kingdom

⁴⁷ Department of Physics, University of Warwick, Coventry, United Kingdom

⁴⁸ STFC Rutherford Appleton Laboratory, Didcot, United Kingdom

⁴⁹ School of Physics and Astronomy, University of Edinburgh, Edinburgh, United Kingdom

⁵⁰ School of Physics and Astronomy, University of Glasgow, Glasgow, United Kingdom

⁵¹ Oliver Lodge Laboratory, University of Liverpool, Liverpool, United Kingdom

⁵² Imperial College London, London, United Kingdom

⁵³ School of Physics and Astronomy, University of Manchester, Manchester, United Kingdom

⁵⁴ Department of Physics, University of Oxford, Oxford, United Kingdom

⁵⁵ Massachusetts Institute of Technology, Cambridge, MA, United States

⁵⁶ University of Cincinnati, Cincinnati, OH, United States

⁵⁷ University of Maryland, College Park, MD, United States

⁵⁸ Syracuse University, Syracuse, NY, United States

⁵⁹ Pontifícia Universidade Católica do Rio de Janeiro (PUC-Rio), Rio de Janeiro, Brazil[†]

⁶⁰ Institut für Physik, Universität Rostock, Rostock, Germany[‡]

⁶¹ Celal Bayar University, Manisa, Turkey[‡]

* Corresponding author.

^a P.N. Lebedev Physical Institute, Russian Academy of Science (LPI RAS), Moscow, Russia.

^b Università di Bari, Bari, Italy.

^c Università di Bologna, Bologna, Italy.

^d Università di Cagliari, Cagliari, Italy.

^e Università di Ferrara, Ferrara, Italy.

^f Università di Firenze, Firenze, Italy.

- ^g Università di Urbino, Urbino, Italy.
- ^h Università di Modena e Reggio Emilia, Modena, Italy.
- ⁱ Università di Genova, Genova, Italy.
- ^j Università di Milano Bicocca, Milano, Italy.
- ^k Università di Roma Tor Vergata, Roma, Italy.
- ^l Università di Roma La Sapienza, Roma, Italy.
- ^m Università della Basilicata, Potenza, Italy.
- ⁿ LIFAELS, La Salle, Universitat Ramon Llull, Barcelona, Spain.
- ^o Hanoi University of Science, Hanoi, Viet Nam.
- ^p Institute of Physics and Technology, Moscow, Russia.
- ^q Università di Padova, Padova, Italy.
- ^r Università di Pisa, Pisa, Italy.
- ^s Scuola Normale Superiore, Pisa, Italy.
- ^t Associated to Universidade Federal do Rio de Janeiro (UFRJ), Rio de Janeiro, Brazil.
- ^u Associated to Physikalisches Institut, Ruprecht-Karls-Universität Heidelberg, Heidelberg, Germany.
- ^v Associated to European Organization for Nuclear Research (CERN), Geneva, Switzerland.